Table S1. Summary of the ECO_2RR performances for different Cu-based complexes and Cu metal-organic frameworks (MOFs). All studies were carried out in H-type cells with aqueous electrolyte systems.

Catalysts	Electrolyte	E (V vs. RHE)	C_2H_4 (FE, %)	Ref.
$[CuCl(phen)_2][CuCl_2]$	0.1M $KHCO_3$	-1.2	47	**This work**
$CuCl(phen)_2$	0.1M $KHCO_3$	-1.0	2	4
CuPPh	0.1M $KHCO_3$	-0.96	45	5
$[Cu_2(phen)_2(OH)_2(H_2O)_2]$ $[Cu_2(phen)_2(OH)_2Cl_2]Cl_2 \cdot 6H_2O$	0.1M $CsHCO_3$	-1.25	42	6
$[Cu_2(NTB)_2Cl_2]^{2+}$	0.1M KCl	-1.28	42	7
PcCu-Cu-O	0.1M $KHCO_3$	-1.2	50	8
BIF-102NSs	0.5M $KHCO_3$	-1.0	11	9
CuTAPP	0.5M $KHCO_3$	-1.0	3	10
Cu_2BDC	0.1M KI	-1.3	34	11
Au NN@PCN-222(Cu)	0.1M $KHCO_3$	-1.2	53	12
S-HKUST-1	0.1M $KHCO_3$	-1.3	60	13

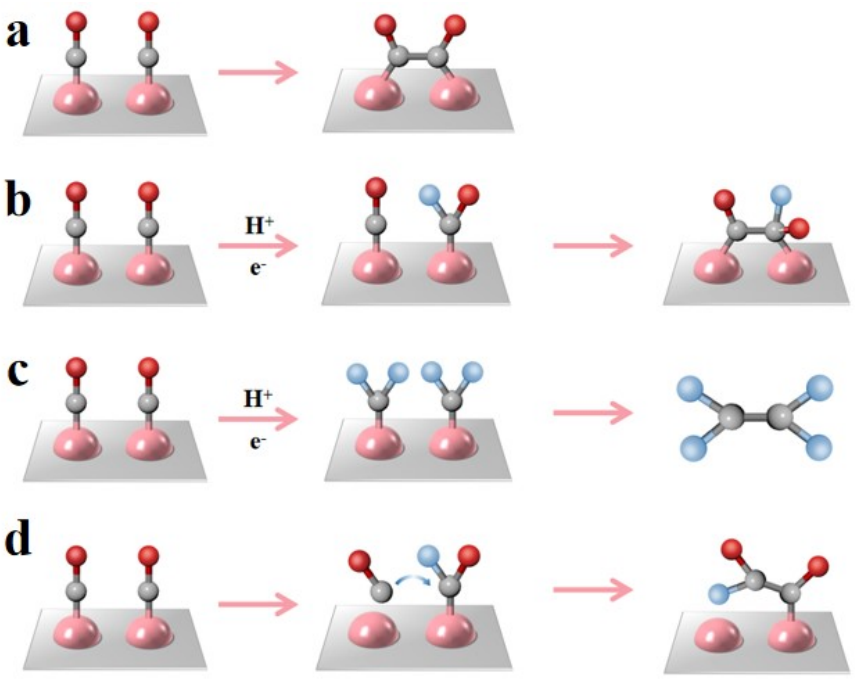

Figure S1. Possible C-C coupling mechanisms in ECO_2RR process. (a, b) Dimerization mechanism. (c) Carbene mechanism. (d) "Insertion of CO in *CHO" mechanism. Noted: Cu, Pink; C, Gray; O, Red; H, Blue.

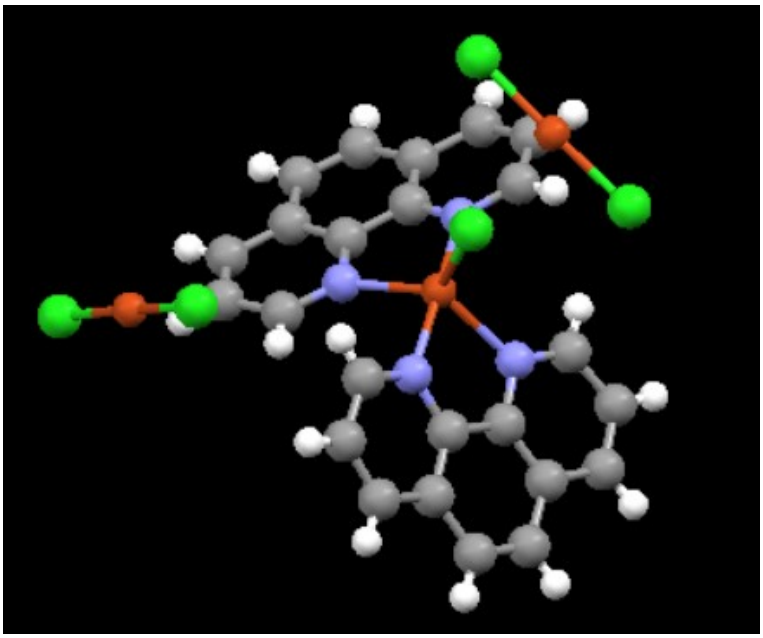

Figure S2. Structure of $[CuCl(phen)_2][CuCl_2]$. Noted: Cu, Orange; Cl, Green; N, Blue; C, Gray; H, White. The $[CuCl(phen)_2]^+$ cation contains a five-coordinated Cu(II) ion, which coordinates with one Cl atom and four N atoms from two phenanthroline (phen) ligands, forming a triangular bipyramidal structure.

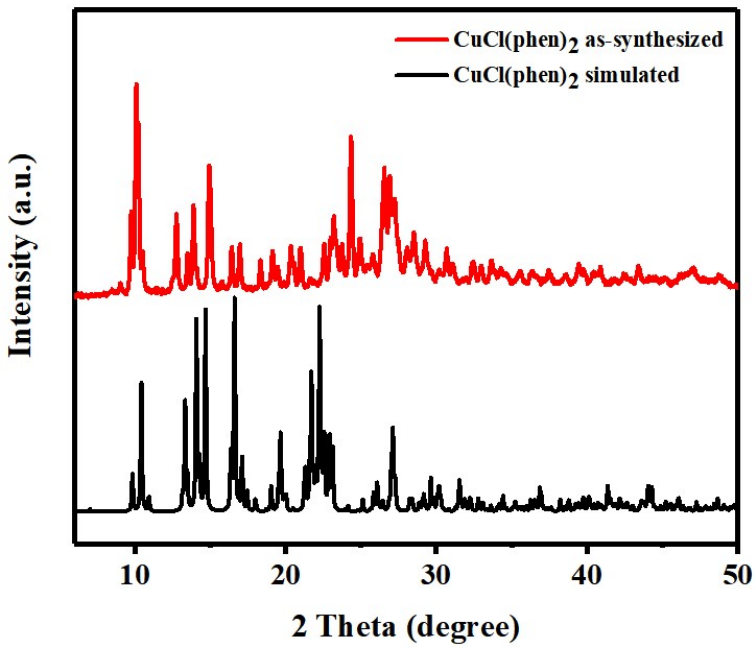

Figure S3. Simulated and as-synthesized XRD patterns of $CuCl(phen)_2$.

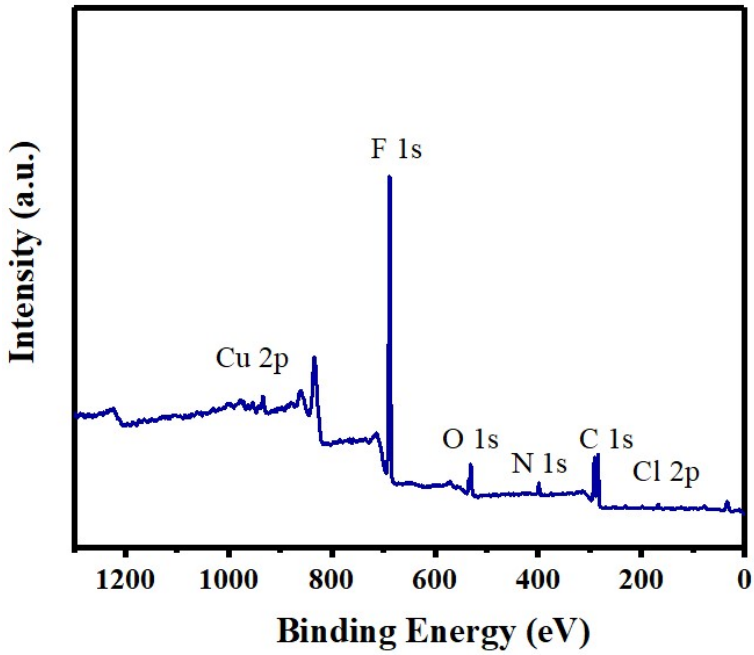

Figure S4. XPS survey spectrum of $[CuCl(phen)_2][CuCl_2]$. The O and F elements in the XPS spectrum are derived from the Nafion solution.

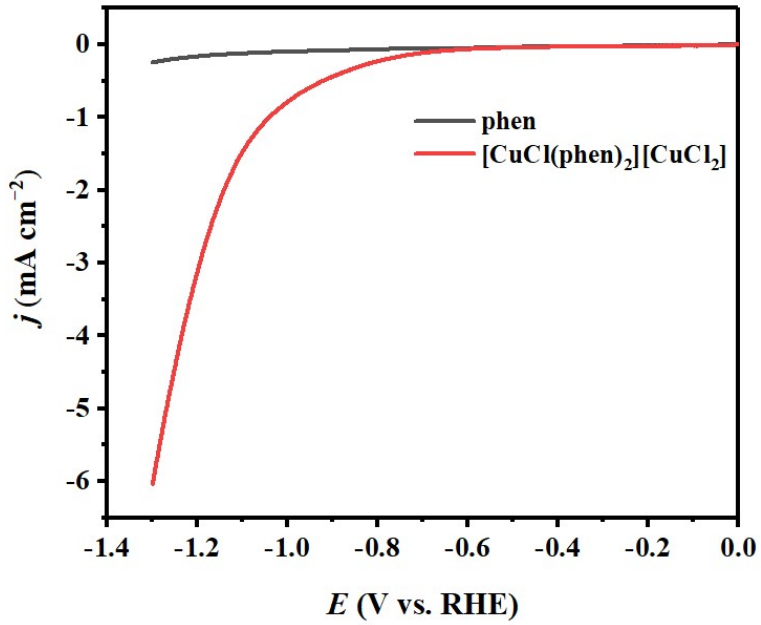

Figure S5. LSV curves of phen and $[CuCl(phen)_2][CuCl_2]$ in CO_2-saturated 0.1 M $KHCO_3$ solution.

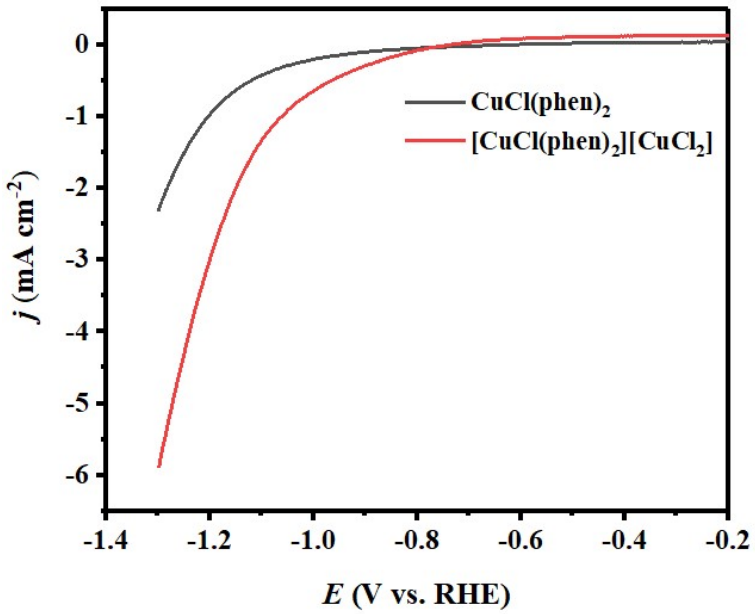

Figure S6. LSV curves of $[CuCl(phen)_2][CuCl_2]$ and $CuCl(phen)_2$ in CO_2-saturated 0.1 M $KHCO_3$ solution.

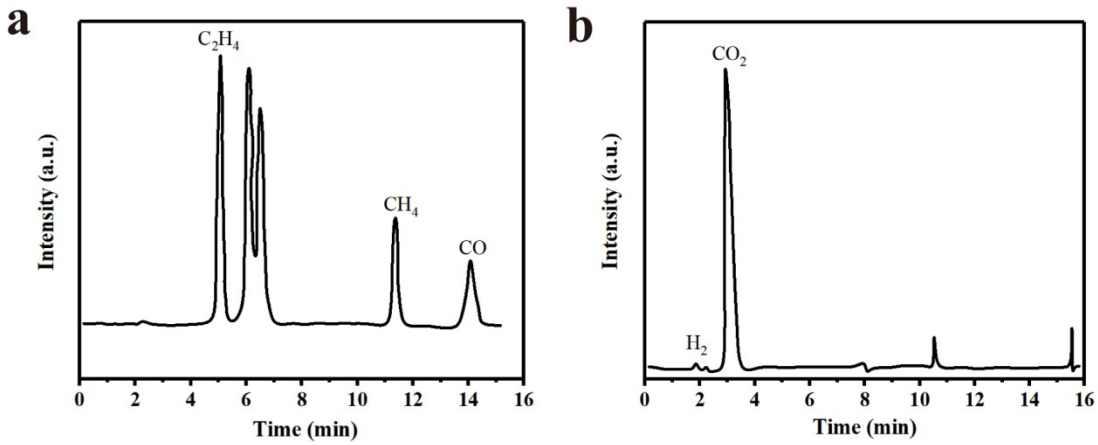

Figure S7. GC profiles of the standard gases with different concentrations. GC spectra peaks of (a) C_2H_4, CH_4 and CO, (b) H_2 and CO_2. The concentrations of C_2H_4, CH_4, CO and H_2 are 222.4, 224.1, 221.6 and 502.4 ppm, respectively.

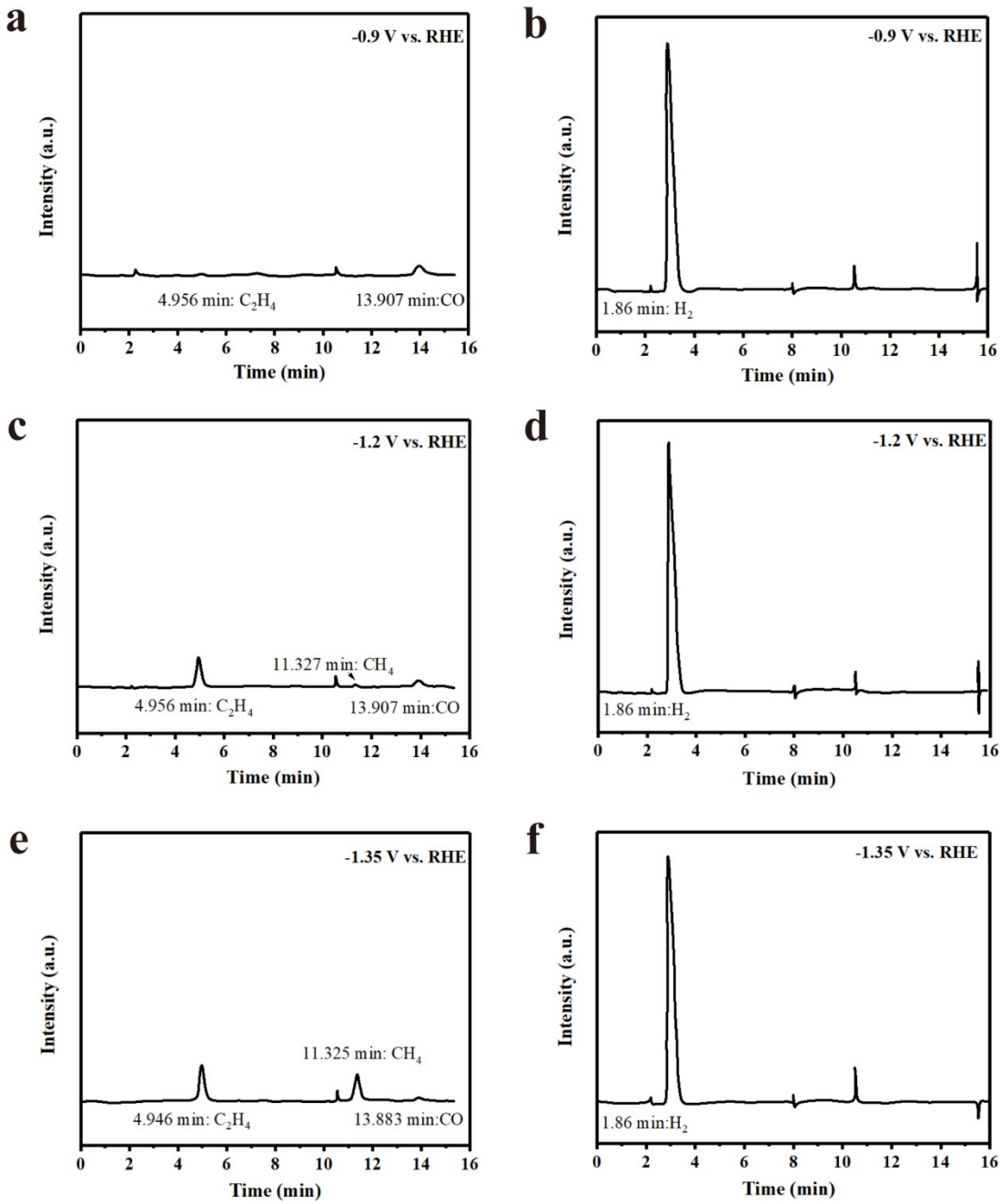

Figure S8. GC profiles of $[CuCl(phen)_2][CuCl_2]$ catalyzing ECO_2RR with different potentials: (a, b) -0.9 V vs. RHE, (c, d) -1.2 V vs. RHE and (e, f) -1.35 V vs. RHE.

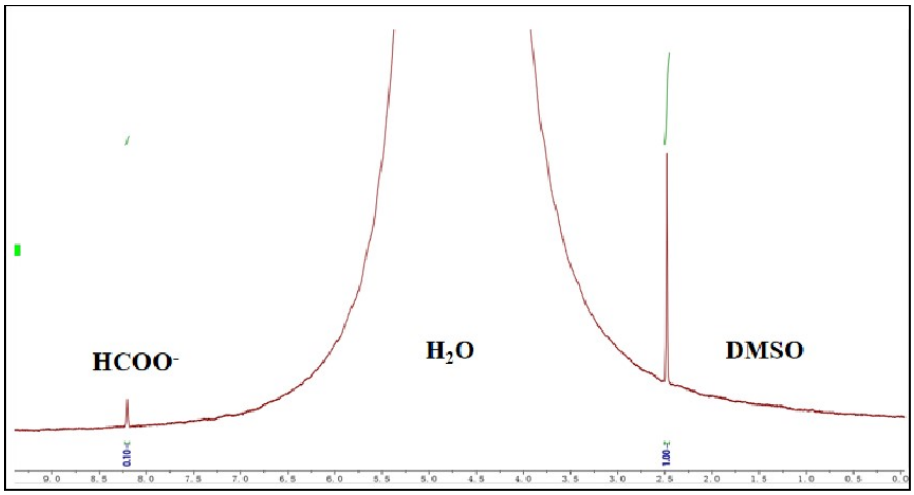

Figure S9. ^{1}H NMR spectrum of the liquid product catalyzed by $[CuCl(phen)_2][CuCl_2]$ at -1.2 V vs. RHE after the ECO_2RR test. The concentration of liquid product was measured using an internal standard, DMSO.

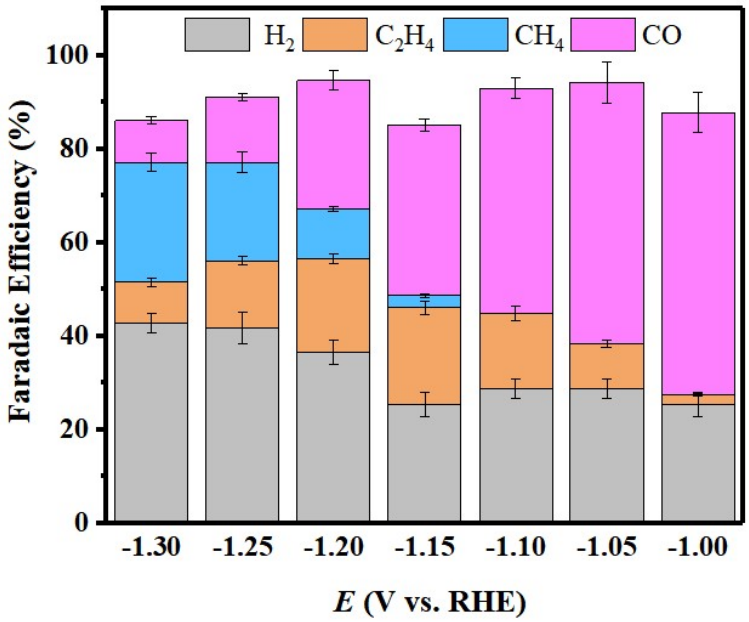

Figure S10. FEs of different reduced gasous products on $CuCl(phen)_2$ catalyst at different potentials.

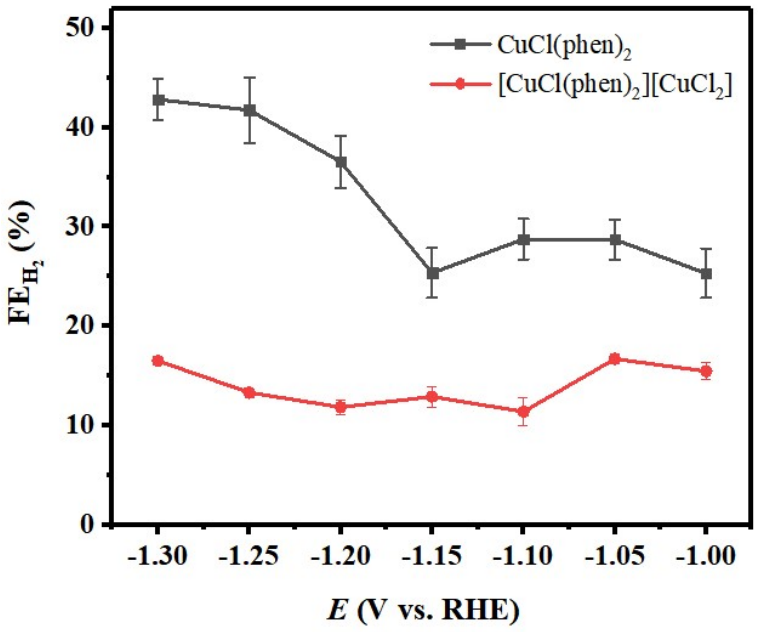

Figure S11. FE_{H2} of $[CuCl(phen)_2][CuCl_2]$ and $CuCl(phen)_2$ at different potentials.

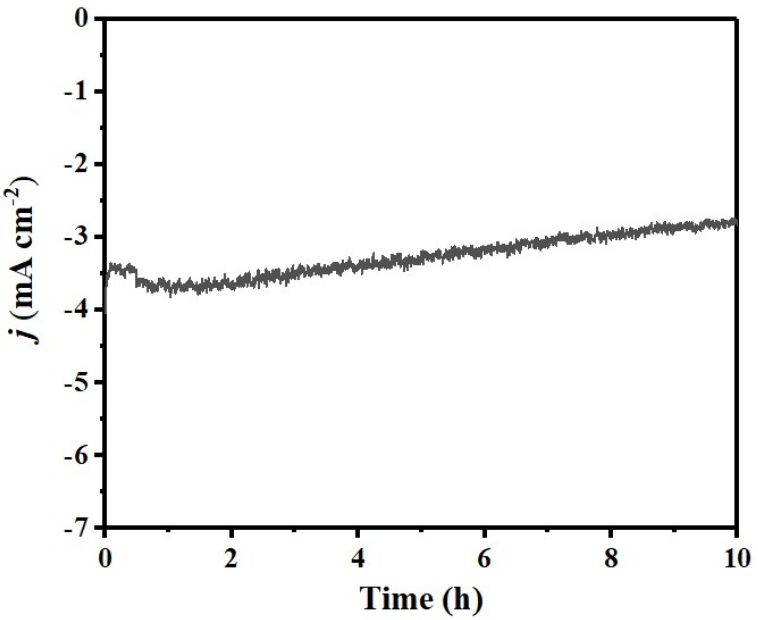

Figure S12. Continuous i-t curve of $[CuCl(phen)_2][CuCl_2]$ at -1.2 V vs. RHE.

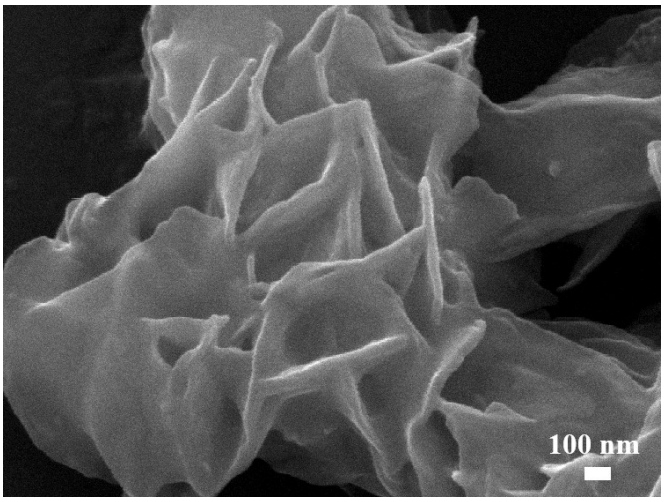

Figure S13. SEM image of $[CuCl(phen)_2][CuCl_2]$ after the ECO_2RR.

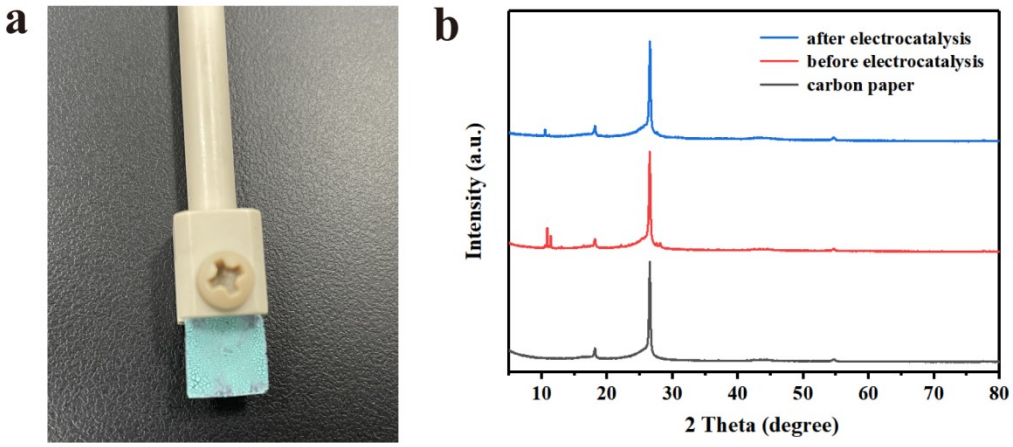

Figure S14. (a) Photograph of $[CuCl(phen)_2][CuCl_2]$ dripping on carbon paper. (b) XRD patterns of $[CuCl(phen)_2][CuCl_2]$ dripping on carbon paper before and after the ECO_2RR tests and blank carbon paper.

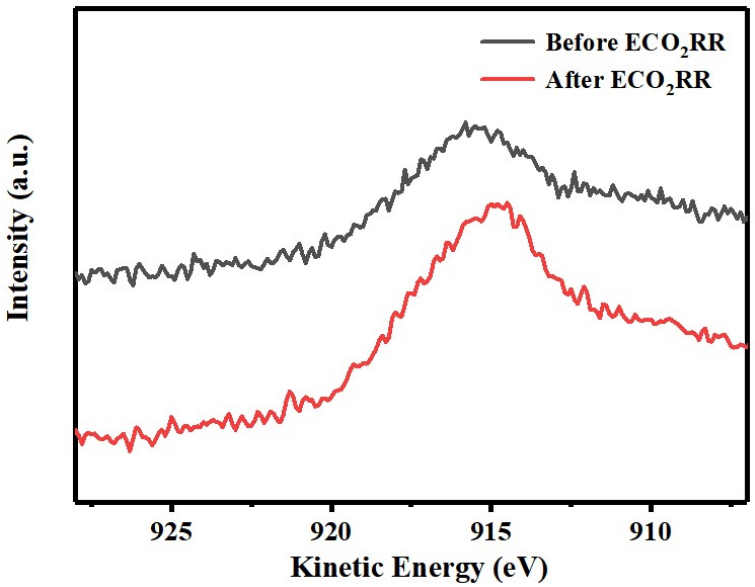

Figure S15. Cu Auger spectrum of $[CuCl(phen)_2][CuCl_2]$ before and after the ECO_2RR test at -1.2 V vs. RHE. The shift of Cu Auger peak towards lower kinetic energy after ECO_2RR, which indicates an increase in electron cloud density, signifying the reduction from Cu(II) to Cu(I). Meanwhile, the narrowing of Auger peak width implies more homogeneous chemical state of Cu species after the ECO_2RR test.